X-ray structure of a ClC chloride channel at 3.0 Å reveals the molecular basis of anion selectivity

Raimund Dutzler*, Ernest B. Campbell*, Martine Cadene†, Brian T. Chait† & Roderick MacKinnon*

*Howard Hughes Medical Institute, * Laboratory of Molecular Neurobiology and Biophysics, and † Laboratory of Mass Spectrometry and Gaseous Ion Chemistry, Rockefeller University, 1230 York Avenue, New York, New York 10021, USA*

The ClC chloride channels catalyse the selective flow of Cl^- ions across cell membranes, thereby regulating electrical excitation in skeletal muscle and the flow of salt and water across epithelial barriers. Genetic defects in ClC Cl^- channels underlie several familial muscle and kidney diseases. Here we present the X-ray structures of two prokaryotic ClC Cl^- channels from *Salmonella enterica* serovar *typhimurium* and *Escherichia coli* at 3.0 and 3.5 Å, respectively. Both structures reveal two identical pores, each pore being formed by a separate subunit contained within a homodimeric membrane protein. Individual subunits are composed of two roughly repeated halves that span the membrane with opposite orientations. This antiparallel architecture defines a selectivity filter in which a Cl^- ion is stabilized by electrostatic interactions with α-helix dipoles and by chemical coordination with nitrogen atoms and hydroxyl groups. These findings provide a structural basis for further understanding the function of ClC Cl^- channels, and establish the physical and chemical basis of their anion selectivity.

Potassium, sodium, calcium and chloride ions are used ingeniously by living systems in the performance of fundamental cellular tasks. Through the action of ion pumps, a large fraction of a cell's metabolic energy is spent establishing transmembrane ion gradients. These gradients, through the action of ion channels, are used to produce electrical signals, activate signal transduction pathways, regulate cell volume, and mediate fluid and electrolyte transport. To carry out these tasks, an ion channel has to be selective, that is, permit only certain ionic species to flow through its pore. Much is known about a very large family of cation channels, which includes the K^+, Na^+, Ca^{2+}, cyclic nucleotide-gated, and several other cation channels. The structure of one of its members, a K^+ channel, reveals cation-selective architectural features that are probably shared by all family members[1,2].

Much less is known about the mechanisms of ion selectivity in anion channels. The ClC Cl^- channels, members of a large family of anion channels, are found throughout biology in both prokaryotic and eukaryotic cells[3–5]. In many cases the biological roles of ClC Cl^- channels are unknown, but in vertebrates several important functions are well established. In skeletal muscle, ClC Cl^- channels stabilize the resting membrane potential and regulate electrical excitability[6]. In the kidney, ClC Cl^- channels operate in concert with the Na^+, K^+, Cl^- cotransporter and K^+ channels to produce transepithelial fluid and electrolyte transport[3,4]. Genetic defects of

Table 1 Summary of data collection and refinement statistics

Data collection	Beamline	Resolution (Å)	Completeness (%)	R_{merge}	$I/\sigma I$
StClC *C*2					
Native	BNL X25	35—3.5	99.7 (100)	5.2 (56.5)	20.0 (2.2)
Pt1	BNL X25	35—5.0	84.8 (81.3)	4.6 (19.0)	14.7 (3.9)
Pt2	BNL X25	35—4.2	99.3 (98.7)	6.1 (31.5)	14.8 (3.0)
Br^-	BNL X25	35—4.5	86.4 (80.0)	5.7 (30.8)	15.2 (3.1)
EcClC $P2_12_12_1$					
Native	ESRF ID13	50—3.5	98.6 (91.3)	7.5 (50.5)	26.3 (1.8)
Se-Met	ESRF ID13	30—4.0	95.1 (97.5)	8.4 (40.5)	17.7 (5.7)
StClC $P2_1$					
Native	BNL X25	35—3.0	94.7 (96.6)	6.5 (54.4)	13.7 (1.7)

Phasing	R_{cullis} (acentric/centric)	Phasing power (acentric/centric)	No. of (sites)	Resolution (Å)
Pt1	0.72/0.78	1.89/1.46	2	35—5.0
Pt2	0.84/0.84	1.24/1.15	2	35—4.2

Refinement	Asymmetric unit, no. of subunits	Resolution (Å)	R_{free}/R_{cryst}	r.m.s.d.* (bond/angles)
E. coli $P2_12_12_1$	6	20—3.5	30.2/29.0	0.01/1.6
S. typhimurium $P2_1$	4	20—3.0	28.8/25.5	0.01/1.5

Data sets of the *C*2 ($a = 191$, $b = 99$, $c = 82$, $\alpha = \gamma = 90°$, $\beta = 98.7°$) and the $P2_1$ ($a = 185$, $b = 90$, $c = 81$, $\alpha = \gamma = 90°$, $\beta = 98.9°$) crystal form of StClC were collected at Brookhaven National Laboratory (BNL), station X25, with the Brandeis-CCD detector. Data sets of the $P2_12_12_1$ ($a = 105$, $b = 152$, $c = 263$, $\alpha = \beta = \gamma = 90°$) crystal form of EcCLC were collected at the European Synchrotron Radiation Facility (ESRF), station ID-13, with a MAR-CCD detector. Numbers in parentheses correspond to the highest resolution shell.
* Root mean square difference.

© 2002 Macmillan Magazines Ltd

human ClC Cl^- channels underlie autosomal dominant and recessive forms of familial myotonia and several familial nephropathies including Bartter's syndrome and Dent's disease[3,4,6].

The study of ClC channels began about 20 years ago when Miller discovered a Cl^- channel from the electric organ of the torpedo ray (ClC-0)[7]. On the basis of quantitative single channel analysis, he predicted that these channels contain two parallel, independent pores (a double-barrel channel)[8,9]. Jentsch cloned the gene for ClC-0, setting the stage for characterization of the entire ClC gene family[10]. Mutational, biochemical and electron microscopic structural analyses confirmed the presence of a double-barrel channel[11–15]. Many other properties of ClC Cl^- channels have been more difficult to discern in the absence of high-resolution structural data. For example, it has been difficult to define many aspects of the membrane topology, and the molecular components of the pore and selectivity filter have remained ambiguous. Different ClC Cl^- channels exhibit unique functional properties, particularly with respect to the signals that cause them to open and close (the process called gating), but they all seem to share two characteristics that are apparently inherent to this ion channel family. The first characteristic is anion over cation selectivity, manifest as permeation by the halogen ions Cl^- and Br^- (and in some cases I^-), and

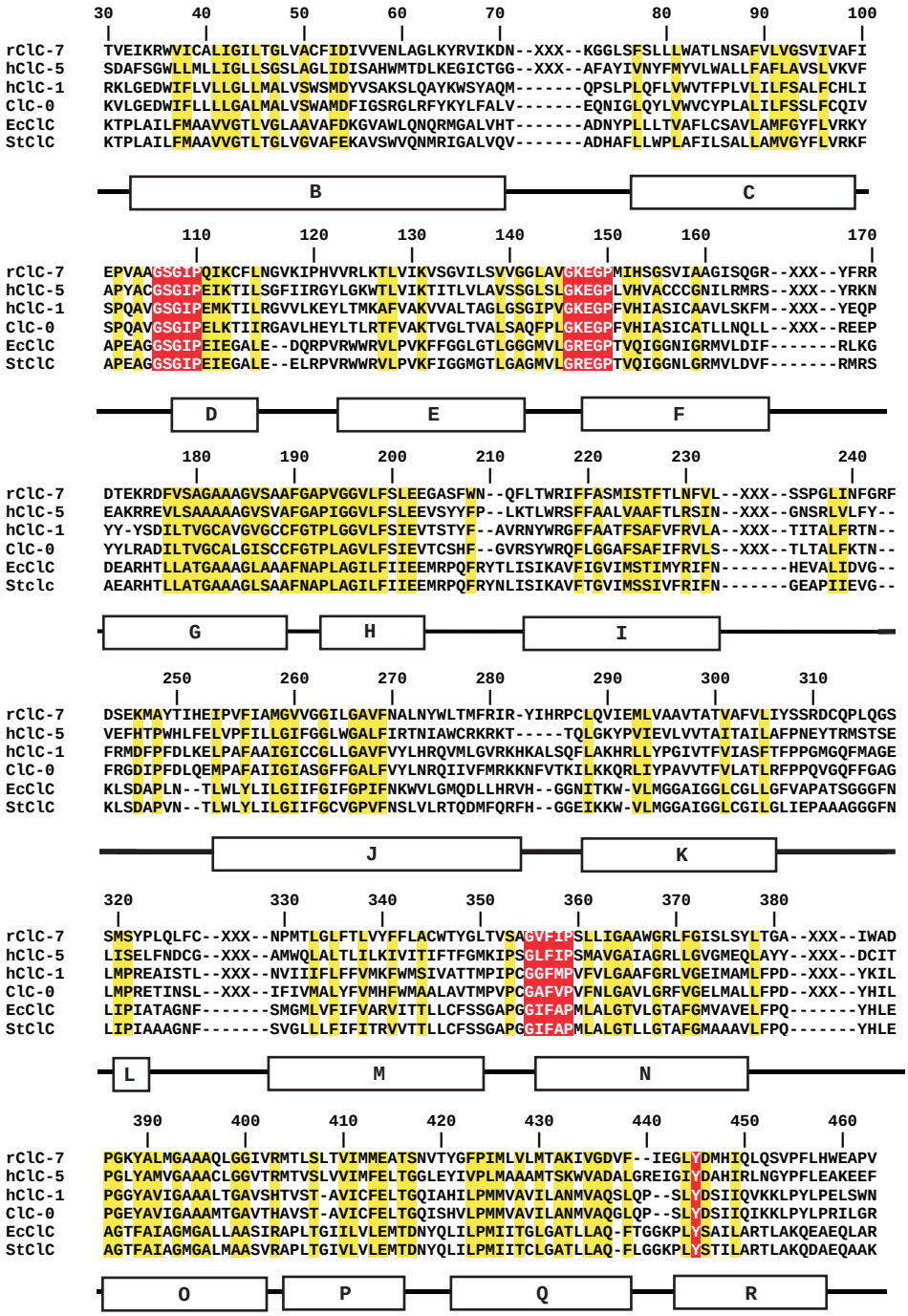

Figure 1 Sequence alignment of ClC channels. Secondary structure and numbering (*S. typhimurium*, StClC channel) are indicated below and above the sequences, respectively. Residues from the Cl^- selectivity filter are red and regions of high homology are yellow. Insertions in eukaryotic ClC channels that are larger than ten residues (XXX) were cut out of the alignment. Amino-acid sequences are: rClC-7, *Rattus norvegicus* (GenBank number Z67743); hClC-5, *Homo sapiens* (NM_000084); hClC-1, *H. sapiens* (M97820); ClC-0, *Torpedo marmorata* (X56758); EcClC, *E. coli* (NC_000913); StClC, *S. typhimurium* (AE008704). The alignment was made with ClustalW[49] followed by manual adjustment.

© 2002 Macmillan Magazines Ltd

block of Cl^- current by larger anions such as I^-, SCN^- and other organic anions[16–18]. The second characteristic of ClC Cl^- channels is strong functional coupling between ion conduction and gating[17,19–23]. The Cl^- ion is the current-carrying substrate that flows through the pore, and it is also an allosteric regulator of the channel's gates. Apparently by binding in the pore, the Cl^- ion influences the open probability, giving rise to properties such as voltage-dependent gating in some ClC Cl^- channels[20,21].

Amino-acid sequences of the integral membrane component of several ClC Cl^- channels are shown in Fig. 1, along with the secondary structure elements defined in the present study. All ClC Cl^- channels exhibit sequence conservation throughout, indicating conservation of their three-dimensional structures. Prokaryotic ClC Cl^- channels depart from eukaryotic family members in the composition of their cytoplasmic amino and carboxy termini (terminal sequences not shown)[24]. Little is known about the biology of prokaryotic ClC Cl^- channels. But given their sequence conservation, together with a recent study of ion selectivity in a ClC Cl^- channel from *E. coli*, we can be certain that a common set of ion selectivity principles applies to the entire family[25].

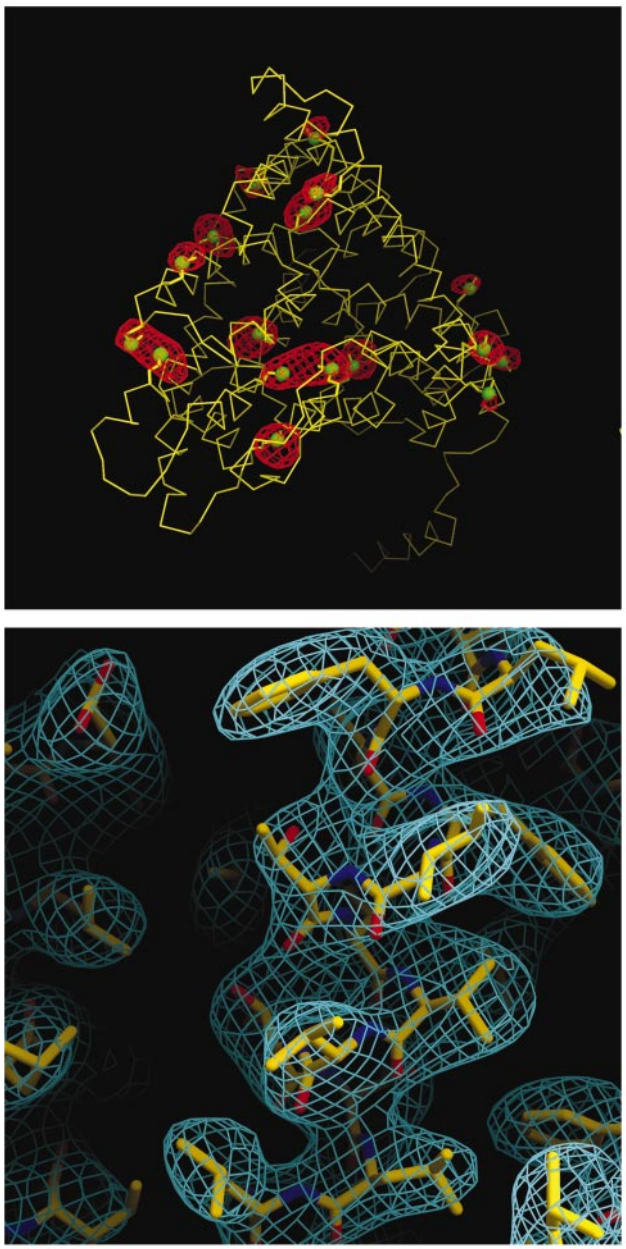

Figure 2 Experimental electron density. **a**, $F_{Se} - F_{native}$ difference density (contoured at 4σ) in the EcClC $P2_12_12_1$ crystal form superimposed on an α carbon trace of the EcClC subunit viewed from outside the cell. Side chains of methionine residues are shown in stick representation with the position of the Se atom indicated by a green sphere. The difference Fourier map was calculated to 4.0 Å and averaged over the six subunits in the asymmetric unit. **b**, Electron density map from the StClC $P2_1$ crystal form at 3.0 Å resolution, contoured at 1σ. The map was calculated from native amplitudes and solvent-flattened, averaged phases. The refined structure is shown as a stick model. Figures 2–6 were prepared with DINO (http://www.dino3d.org).

Structure

The structures of two ClC Cl^- channels from *S. typhimurium* (StClC) and *E. coli* (EcClC) were determined in parallel with data to 3.0 and 3.5 Å Bragg spacings, respectively (Table 1 and Methods). Initial phases were estimated from platinum derivatives of StClC crystals. The building and refinement of accurate atomic models were aided by the identification of 17 methionine residues in selenium difference maps of the EcClC channel (Fig. 2a) and by the presence of two-fold, four-fold and six-fold noncrystallographic symmetry (NCS) in a variety of crystal forms. The NCS was used to provide accurate phases for the calculation of electron density maps and to constrain the atomic coordinates throughout refinement[26] (Fig. 2b).

Two views of the StClC Cl^- channel are shown in Fig. 3. The channel contains two identical subunits (red and blue), which are related by a two-fold axis of symmetry perpendicular to the membrane plane. Viewed along the two-fold axis from outside the cell, each subunit is triangular (Fig. 3a). The entire channel with two subunits is shaped like a rhombus, with major and minor diagonals of 100 and 55 Å, respectively. In the direction perpendicular to the membrane plane, the channel is about 65 Å thick owing to helical extensions that protrude into the aqueous solution (Fig. 3b). The contact surface area between subunits is extensive, encompassing nearly 2,300 $Å^2$ within the membrane. Such a large, stable interface is expected because ClC Cl^- channels are thought to exist and function only as dimers. The pore, or ion pathway, is not formed at the interface between subunits. Rather, each subunit forms its own independent pore and selectivity filter (green sphere). With regard to their pore stoichiometry, ClC Cl^- channels are like the porins[27], the aquaporins[28,29] and bacteriorhodopsin[30], not like the cation channel family to which the K^+ channels belong. The former examples are trimers or tetramers of identical subunits in which each individual subunit forms an independent pore or active site. The K^+ channels, however, are tetramers in which the pore is formed by four identical subunits encircling a central ion pathway[1].

The structure of the EcClC channel is essentially the same as the StClC channel, except where deviations occur on the surface owing to crystal contacts. Likewise, deviations from perfect two-fold symmetry between the subunits within the dimeric channel probably result from protein contacts within the crystal. For example, the N terminus from only one of the subunits is visible as an α-helix near the cytoplasmic surface, whereas in the other subunit the N terminus is disordered (Fig. 3).

The ClC Cl^- channel subunit contains 18 α-helices (labelled A–R) and exhibits a complex topology (Fig. 4a). The three-dimensional structure reveals an internally repeated pattern in the sense that the N-terminal half of the polypeptide (α-helices B–I, green) is structurally related to the C-terminal half (J–Q, blue). The two similar structures have opposite orientations in the membrane, that is, they run antiparallel, and create a pseudo two-fold symmetry axis within the membrane. The internal symmetry is easily appreciated when viewing a subunit along the pseudo two-fold axis from the dimer interface (Fig. 4b). We refer to this arrangement as an antiparallel architecture. The internal repeat pattern in ClC Cl^- channels was not previously recognized on the basis of amino-acid sequence analysis, but careful alignment with knowledge of the protein structure shows that the two halves are indeed weakly correlated in their sequence, particularly with respect to

© 2002 Macmillan Magazines Ltd

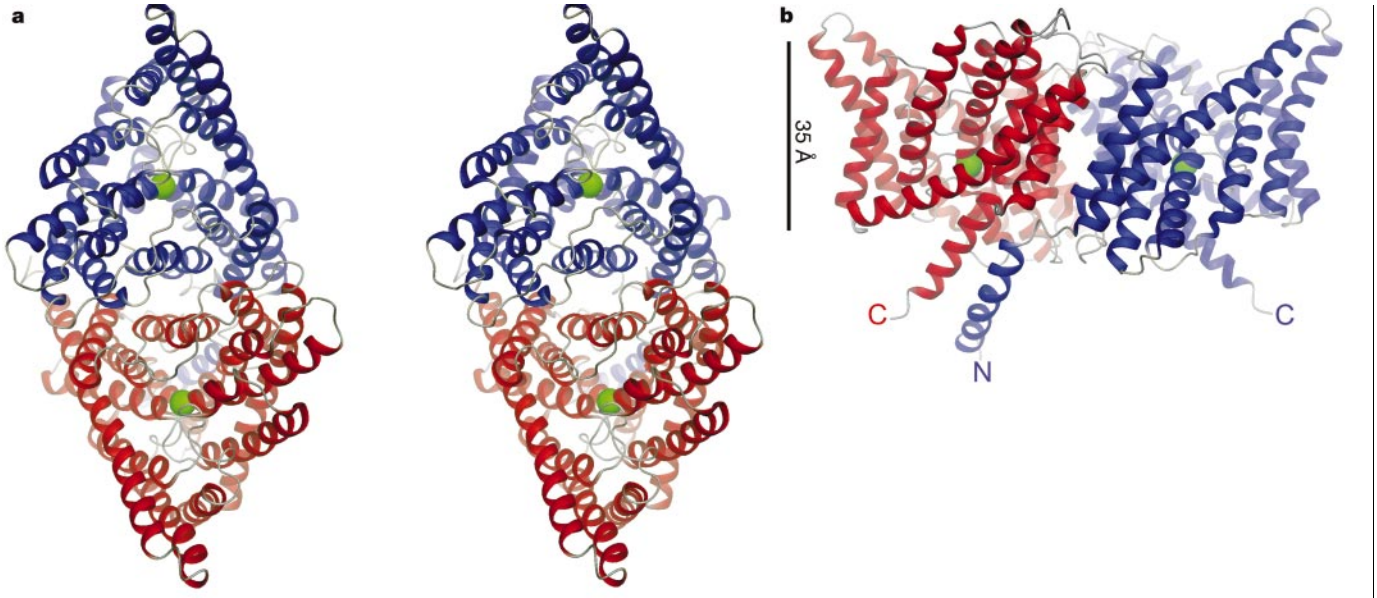

Figure 3 Structure of the StClC dimer. **a**, Stereo view of a ribbon representation of the StClC dimer from the extracellular side. The two subunits are blue and red. A Cl^- ion in the selectivity filter is represented as a green sphere. **b**, View from within the membrane with the extracellular solution above. The channel is rotated by 90° about the *x*- and *y*-axes relative to **a**. The black line (35 Å) indicates the approximate thickness of the membrane. See Supplementary Information for the X-ray structure.

the disposition of glycine residues. It is interesting that an antiparallel architecture is also seen in the individual subunits of aquaporins (channels for water and small solute molecules), even though their membrane-spanning topology is unrelated to that of ClC Cl^- channels[28,29].

The transmembrane α-helices within a ClC subunit are remarkably tilted and variable in length (Fig. 4b). There is an important reason underlying this seemingly complicated arrangement of helices. The two halves of the subunit (Fig. 4b, green and blue) wrap around a common centre so as to bring together amino acids at the ends of α-helices from disparate segments of the polypeptide chain (Figs 1 and 4b, red). As we show below, these amino acids form the Cl^- ion selectivity filter within the membrane.

Anion selectivity

Important amino acids from four separate regions are brought together near the membrane centre to form an ion-binding site. These regions (red in the sequence alignments, Fig. 1) are highly conserved in ClC Cl^- channels; they include the sequences GSGIP (106–110), G(K/R)EGP (146–150) and GXFXP (355–359), as well as Tyr 445. It is significant that these sequences occur at the N termini of α-helices, where polypeptide loops precede α-helices D, F and N (Figs 1 and 4a). As a result, each of these helices is oriented with its N terminus pointed towards the binding site. Because of the helix dipole, or N-terminal positive end charge, this arrangement of helices is expected to create an electrostatically favourable environment for anion binding (depicted by blue in Fig. 5a).

A strong peak of electron density is present in the ion-binding site in solvent-flattened, averaged experimental maps (not shown). To determine whether the peak is due to a bound Cl^- ion, we took advantage of the fact that ClC Cl^- channels conduct Br^- ions nearly as well as Cl^- ions. We grew crystals in a solution containing NaBr instead of NaCl. The experiment was carried out using a *C*2 crystal form (Table 1). Difference electron density corresponding to Fourier coefficients $F_{Br} - F_{Cl}$ (Fig. 5b, red) is shown superimposed on a $2F_o - F_c$ electron density map surrounding the corresponding position within the $P2_1$ crystal form (Fig. 5b, cyan). The strong positive difference peak is consistent with the replacement of a Cl^- ion by the more electron-dense Br^- ion. We therefore conclude that the ion present at this site is indeed a Cl^- ion. Because this site is formed by the most conserved amino acids in the ClC Cl^- channel family and contains a Cl^- ion, we conclude that it is the selectivity filter.

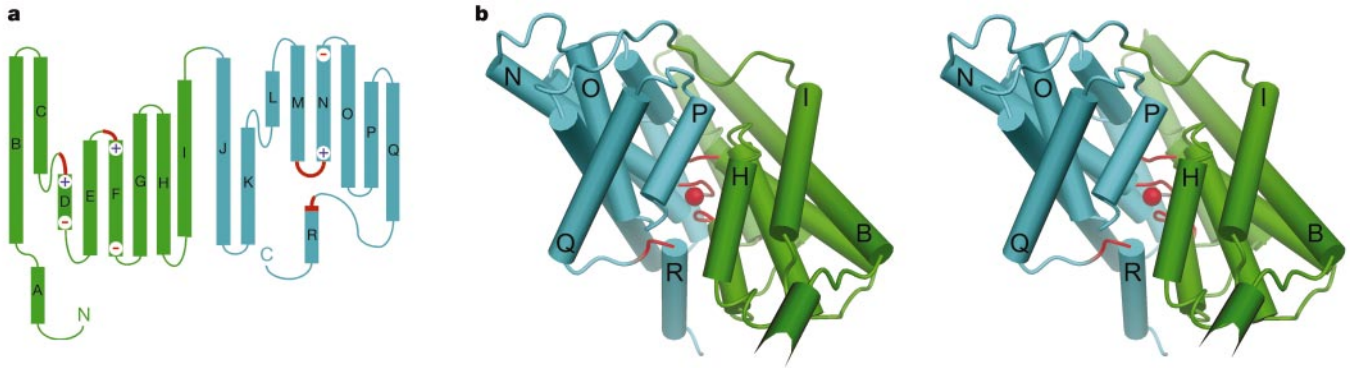

Figure 4 Structure of the StClC subunit. **a**, The α-helices (A–R) are drawn as cylinders with the extracellular region above and the intracellular region below. The two halves of the subunit are green and cyan, and regions forming the Cl^- selectivity filter are red. Partial charges at the end of helices involved in Cl^- binding are indicated by + and – (end charges) to indicate the sense of the helix dipole. **b**, Stereo view of the StClC subunit viewed from within the plane of the membrane from the dimer interface with the extracellular solution above. The α-helices are drawn as cylinders, loop regions as cords (with the selectivity filter red), and the Cl^- ion as a red sphere.

© 2002 Macmillan Magazines Ltd

The Cl^- ion is coordinated by main-chain amide nitrogen atoms from amino acids Ile 356 and Phe 357 and by the side-chain oxygen atoms from Ser 107 and Tyr 445 (Figs 1 and 5c). The nitrogen atoms are not involved in hydrogen bonding with the protein, and are available for ion binding because α-helix N begins just at position 356, allowing the 'free' pair of amide nitrogen atoms to form a cradle on one side of the Cl^- ion. The side chains of Ser 107 and Tyr 445 contact the Cl^- ion opposite the nitrogen cradle. The electrophilic aromatic ring makes the Tyr hydroxyl group a good proton donor and therefore an excellent Cl^- ion ligand. Likewise, the Ser 107 hydroxyl group is a good ligand because it caps the end of α-helix D. That is, by forming a hydrogen bond with the amide nitrogen of Ile 109, the serine hydroxyl is polarized to interact more strongly with the Cl^- ion. In addition to the interactions with polar functional groups, the Cl^- ion is surrounded by a number of hydrophobic amino-acid side chains.

It is noteworthy that in the Cl^- channel the ion does not make direct contact with a full positive charge from lysine or arginine residues. The favourable electrostatic environment for Cl^- arises instead from partial positive charges contributed by helix dipole interactions and by contacts with main-chain and side-chain nitrogen and oxygen atoms. We suggest that a full positive charge would create a deep energy well and cause a Cl^- ion to bind too tightly. Thus, it would appear that evolution of the channel has resulted in partial charges to stabilize a Cl^- ion and still permit rapid ionic diffusion rates.

Conduction pore

The Cl^- ion conduction pore is shown in Fig. 6a, viewed from within the membrane with the extracellular solution above and the intracellular solution below. The picture was made by cutting the subunit in half along a plane that is perpendicular to the pseudo two-fold axis. The N termini of pseudo symmetry-related α-helices F and N, together with that of D, point at a narrow tunnel, about 12 Å long, towards the centre of the membrane. Wider, water-filled vestibules reach in from the extracellular and intracellular solutions (Fig. 6a, blue mesh). The Cl^- ion is shown at its position in the pore, about 2 Å below the pseudo two-fold axis. Unexpectedly, just above the pseudo two-fold axis, a glutamate side chain projects into the pore. Glu 148, a rather conserved residue in ClC Cl^- channels, is sandwiched between the positive ends of α-helices F and N, hydrogen bonded to its own amide nitrogen atom. The selectivity filter effectively has two anions in it, a Cl^- ion closer to the intracellular vestibule (inner site) and a carboxylate anion closer to the extracellular vestibule (outer site). For Cl^-conduction to occur, the glutamate side chain presumably would have to swing out of the way (perhaps associated with structural changes extending beyond the glutamate side chain), permitting the entry of a Cl^- ion in its place.

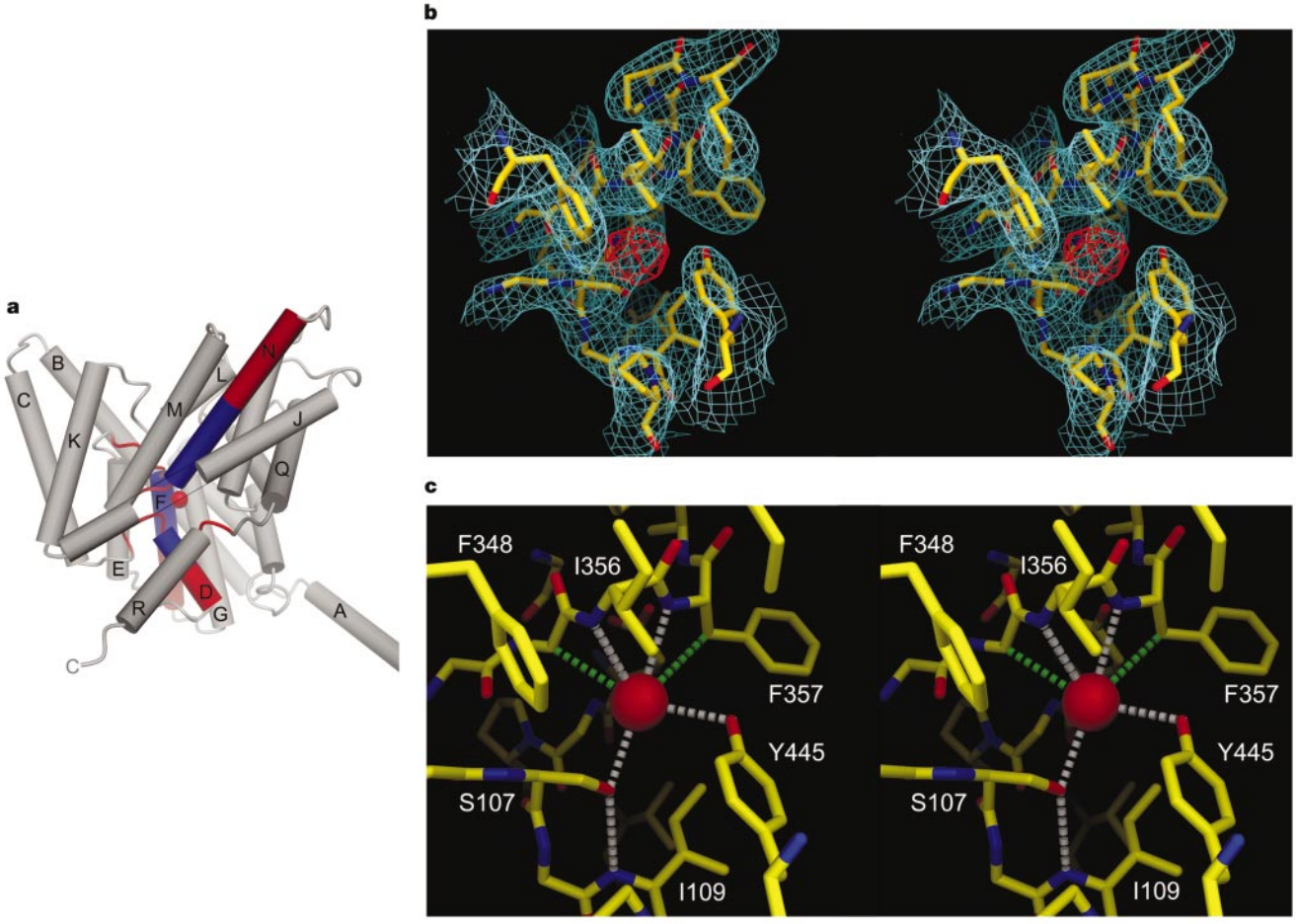

Figure 5 Structure of the StClC selectivity filter. **a**, Helix dipoles (end charges) point towards the selectivity filter. The α-helices are shown as cylinders with labels corresponding to Fig. 4a. The amino (positive, blue) and carboxy (negative, red) ends of α-helices D, F and N are shown. The selectivity filter residues are shown as red cords surrounding a Cl^- ion (red sphere). The view is from 20° below the membrane plane; the dimer interface is to the right, and the extracellular solution above. Part of α-helix J has been removed for clarity (grey line). **b**, Stereo view of electron density in the selectivity filter. A $2F_o - F_c$ Cl^- omit map (StClC $P2_1$ crystal form, 3.0 Å resolution, 1σ contour, cyan) is superimposed on a stick model of residues selected within a 5 Å radius of the Cl^- ion. An $F_{Br} - F_{Cl}$ difference Fourier map (StClC $C2$ crystal form, 4.5 Å resolution, 5σ contour, red) is shown transformed to the corresponding position in the $P2_1$ unit cell. **c**, Stereo view of the Cl^- ion-binding site. Distances (<3.6 Å) to the Cl^- ion (red sphere) are shown for polar (white dashed lines) and hydrophobic (green dashed lines) contacts. A hydrogen bond between Ser 107 and the amide nitrogen of Ile 109 is shown (white dashed line).

© 2002 Macmillan Magazines Ltd

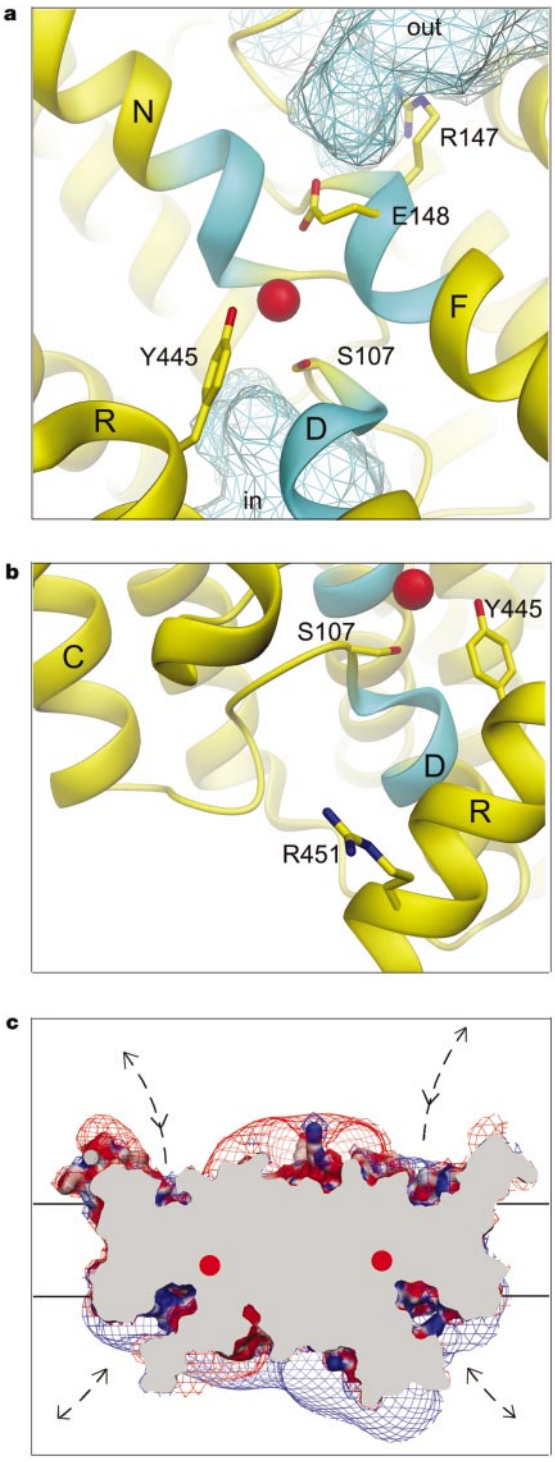

Figure 6 Ion conduction pathway. **a**, The ion-binding site viewed from the dimer interface, along the pseudo two-fold axis, with foreground α-helices removed for clarity. The protein is shown as a ribbon with selected residues as sticks. The amino terminal ends of α-helices D, F and N are cyan and Cl^- is shown as a red sphere. Aqueous cavities approaching the selectivity filter from the extracellular solution (out) and intracellular solution (in) are shown as a cyan mesh. **b**, View of the intracellular channel entrance. The molecule is rotated by about 90° around the *y*-axis relative to **a**. **c**, Surface electrostatic potential on the ClC dimer in 150 mM electrolyte. The channel is sliced in half to show the pore entryways (but not the full extent of their depth) on the extracellular (above) and intracellular (below) sides of the membrane. Isocontour surfaces of −12 mV (red mesh) and +12 mV (blue mesh) are shown. Cl^- ions are shown as red spheres. Dashed lines highlight the pore entryways. The solvent-excluded surface of the StClC dimer was calculated with the program MSMS[50].

The structure of this narrow, anion-selective region of the channel is interesting in light of biophysical studies on the influence of extracellular Cl^- ion concentration on the function of ClC Cl^- channels. Some ClC channels have been described as being Cl^--activated chloride channels, because a certain amount of Cl^- is required in the extracellular solution to gate the pore open[20]. Moreover, Cl^- appears to exert its gating effect by actually entering the pore, meaning that gating (the process of opening the pore) and ion conduction (the process of ions moving through the open pore) are closely linked[20,21]. An additional important piece of information comes from the observation, made in ClC-1 Cl^- channels, that a series of anions rank differently in their effects on conduction and gating[17]. To explain these findings, two anion-binding sites in the pore have been hypothesized, one accounting for 'conduction selectivity' (proposed to be closer to the intracellular solution) and the other for 'gating selectivity' (proposed to be closer to the extracellular solution). The structure offers a possible explanation for these findings. The inner site, where a Cl^- ion is specifically coordinated, probably is important for conduction selectivity as ions diffuse through the open pore. What we are calling the outer site would prevent the channel from conducting as long as the glutamate side chain 'blocks' the ion pathway. However, if Cl^- ions from the extracellular solution can enter the pore and induce a conformational change that displaces the glutamate side chain (that is, by competing with the carboxylate group), then the property of Cl^- activation could be explained. Such a mechanism would imply that when the pore is open, conduction occurs through the interaction of two closely spaced Cl^- ions in the selectivity filter.

The vestibules leading up to the selectivity filter on both sides of the membrane contain basic (positively charged) amino acids, for example Arg 147 (Fig. 6a) and Arg 451 (Fig. 6b). The distribution of charges on the entire channel surface creates an electrostatic potential that probably funnels Cl^- ions into the pore entryways (Fig. 6c). The two pores on the dimer are separated by a large distance and by an electronegative (Cl^--repulsive) region on the extracellular surface (Fig. 6c, red). These features are consistent with the functional independence of the two pores in ClC-0 channels[8].

The effects of numerous mutations on the properties of ClC-0 and ClC-1 Cl^- channels have been studied[3–5]. We mention only a few of these results as they relate to the focus of this paper, the mechanism of anion selectivity. Mutation of serine to threonine at the Cl^- binding site in ClC-0 (Ser 107 of StClC, Figs 1 and 5c) affected selectivity among anions and dramatically reduced conductance[11]. Mutations near the extracellular entryway (StClC 146–148; Figs 1 and 6a) and intracellular entryway (StClC α-helix R, Figs 4b and 6b) of ClC-0 also altered ion conduction as well as gating[12,20,23,31,32]. One site in particular, Lys 519 of ClC-0 (adjacent to Arg 451 of StCLC, Fig. 6b) appears to influence conduction mainly by an electrostatic interaction, whereby the positively charged amino group attracts Cl^- ions and increases the conductance[12,23]. The results of these mutational studies are in good agreement with the X-ray structure.

The location of α-helix R in the structure is intriguing (Figs 4b and 6b). Its N-terminal end begins at the selectivity filter, where Tyr 445 interacts directly with the Cl^- ion, and its C-terminal end projects into the cytoplasm. As a point of speculation, α-helix R would seem to offer a direct route for regulating channel function through processes occurring in the cytoplasm.

Discussion

The ClC Cl^- channel is a homodimer with a two-fold axis perpendicular to the membrane plane; each of the subunits within the dimer forms its own ion-conduction pore. Each individual subunit, or channel-forming unit, exhibits an antiparallel architecture (Fig. 7a). Why did such a structural plan evolve? We propose that the antiparallel architecture satisfies two fundamental physical

© 2002 Macmillan Magazines Ltd

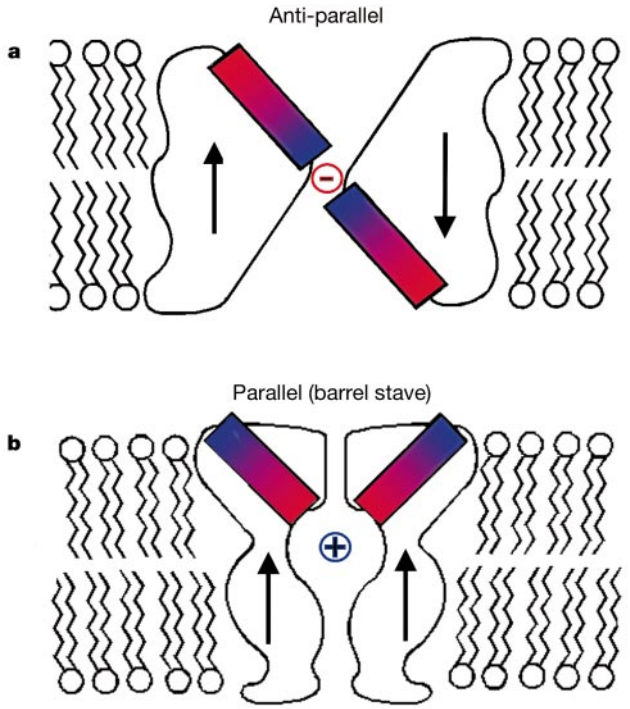

Figure 7 Two architectures for ion-channel proteins. **a**, The antiparallel architecture of ClC Cl^- channels contains structurally similar halves with opposite orientations in the membrane (arrows). This architecture permits like ends (same dipole sense) of α-helices to point at the membrane centre from opposite sides of the membrane (180° separation). **b**, The parallel or barrel stave architecture of K^+ channels contains structurally similar or identical subunits with the same membrane orientation (arrows). Helices point at the membrane centre from the same side of the membrane. Helices are depicted as dipoles with blue (positive) and red (negative) ends.

constraints on membrane-transport proteins. First, active sites or selectivity filters within the membrane exploit the polar ends of α-helices to stabilize (or destabilize) substrates or ions through electrostatic and chemical interactions. Second, the opposite ends of the helices (away from the active site) have to be directed into the aqueous environment outside the membrane. This second constraint stems from the simple fact that it is energetically unfavourable to bury the polar end of a helix in the low-dielectric membrane core. An antiparallel architecture satisfies these constraints elegantly, allowing like helix ends (same dipole orientation) to point at the selectivity filter from opposite directions (with a 180° angular separation, Figs 6a and 7a). There are other ways to satisfy the above constraints on membrane helices and active sites, as in the case of the K^+ channel (Fig. 7b), but the antiparallel architecture is a fascinating solution to the problem.

Anion selectivity is achieved in ClC Cl^- channels through partial positive charges, not through full positive charges. This principle of partial charges is also used in the K^+ channel, but with reversed polarity, in the form of negative helix dipoles and main-chain carbonyl oxygen atoms[1,2]. Partial charges create a favourable electrostatic environment for relatively large monovalent ions such as Cl^- (radius 1.81 Å) or K^+ (radius 1.33 Å) while preventing the ions from binding too tightly—a requirement for high conduction rates. In the ClC Cl^- channels, partial charges are contributed by positive helix dipoles, by main-chain amide nitrogen atoms, and by side-chain hydroxyl groups of serine and tyrosine residues. The amino acids forming the selectivity filter are quite conserved in ClC Cl^- channels, implying that the anion-selective principles described here apply to the entire family.

We wondered about the striking architectural difference between Cl^- and K^+ channels: the Cl^- channel has a roughly hourglass-shaped pore with a narrow constriction (its selectivity filter) near the membrane centre (Fig. 7a), whereas the K^+ channel has a widening, or cavity, at the membrane centre (Fig. 7b). The cavity in K^+ channels, working in concert with helix dipoles, helps to overcome the dielectric barrier, or energy barrier experienced by an ion owing to the low-dielectric membrane environment[1,33]. For some reason the Cl^- channel uses only helix dipoles. Is the membrane dielectric barrier different for K^+ and Cl^- ions? We do not know the full answer, but we do know of one difference that might make the dielectric barrier smaller for anions. Biological membranes have a dipole layer on the plane of the water–lipid interface that contributes a positive electrostatic potential, perhaps as much as +300 mV (ref. 34), to the membrane interior[35,36]. The precise origin of this dipole layer is unknown, but its presence accounts for the fact that hydrophobic anions partition into biological membranes with greater ease than hydrophobic cations[34]. In other words, all else being equal, anions are more stable than cations inside the membrane. Perhaps for this reason Cl^- channels do not require a wide, water-filled pore near the membrane centre to minimize the dielectric barrier.

ClC Cl^- channels are complex; further work will be required to understand how they gate and how the gating processes are coupled to ion conduction through the pore. We have provided here a structural basis for guiding further work on ClC Cl^- channel function, and established the physical and chemical principles underlying ion selectivity in an anion channel. □

Methods

Protein preparation

EcClC (GenBank accession number NC_000913) and StClC (AE008704) were cloned into a pET28b+ vector using *Nco*I and *Xho*I restriction sites and protein expressed with a C-terminal histidine tag in *E. coli* strain BL21 DE3. In StClC, Met 26 was mutated to Leu and Cys 264 was mutated to Val. Homogeneous expression of the full-length protein was confirmed by matrix-assisted laser desorption/ionization mass spectrometry (MALDI-MS). Bacteria were grown to an absorbance at 600 nm (A_{600}) of 1.0 in the presence of 50 mg l^{-1} kanamycin at 37 °C, and induced with 200 μM isopropyl-β-D-thiogalactopyranoside (IPTG) overnight at 25 °C. Cells were centrifuged, lysed by French press or sonication in 50 mM Tris-HCl buffer at pH 7.5, 150 mM NaCl, 200 mg l^{-1} lysozyme, 20 mg l^{-1} DNase, leupeptin and pepstatin, and 1.0 mM phenylmethyl sulphonyl fluoride (PMSF), and extracted with 50 mM *n*-decyl-β-maltoside (Anatrace, Sol-Grade D322S) for 2 h at room temperature. Extract was centrifuged for 40 min at 30,000*g* and the supernatant loaded onto a cobalt-affinity column (Talon Metal Affinity Resin, Clonetech). The column was washed with imidazole (gradient 0–40 mM) and desired protein eluted with 400 mM imidazole. Protein was concentrated to 15–20 mg ml^{-1}, the His tag was removed by proteolytic digestion with 5 international units (IU) thrombin (StClC) or 1.5 IU endoprotease Lys-C (EcClC) for 2 h at room temperature, and protein was then run on a Superdex 200 column in 45 mM *n*-octyl-β-maltoside, 150 mM NaCl and 10 mM Tris-HCl at pH 7.5. Pooled peaks were concentrated to 10–15 mg ml^{-1} and dialysed overnight against 45 mM *n*-octyl-β-maltoside, 75 mM NaCl, 10 mM Tris-HCl at pH 7.5. Protein for Br^- soaks were dialysed against 45 mM *n*-octyl-β-maltoside, 75 mM NaBr and 10 mM Tris-sulphate buffer at pH 7.5. For protein labelled with seleno-L-methionine, transformed bacteria (B834 DE3) were grown in minimal medium (L-methionine replaced by seleno-L-methionine), and the protein was purified as above. Substitution of methionine sulphur with selenium was confirmed by MALDI-MS.

Crystal preparation

Crystals of EcClC and StClC channels were grown in sitting drops at 20 °C by equilibrating a 1:1 mixture of protein and reservoir solutions against the reservoir. For the EcClC $P2_12_12_1$ crystal form (with and without selenium) the reservoir solution contained 31–34% polyethylene glycol (PEG 400), 50 mM Tris at pH 8.5, 50 mM Na_2SO_4 and 50 mM Li_2SO_4. The crystals were frozen in their mother liquor in the cryogenic nitrogen stream. The *C*2 and the $P2_1$ crystal forms of StClC crystallized from the same reservoir solution, which contained 26–31% PEG 400, 50 mM sodium acetate at pH 4.6, 75–100 mM Na_2SO_4 and 75–100 mM Li_2SO_4. PEG 400 was increased to 37% by dialysis before freezing in the nitrogen stream. For derivatization, crystals were soaked for 6 h in mother liquor containing 1 mM Pt(II)-terpyridine chloride (Aldrich).

Crystallography

All data sets were collected on frozen crystals on beam-lines BNL X25 and ESRF ID-19 (Table 1). The data were indexed and integrated with DENZO and SCALEPACK[37] and further processed with the CCP4 programs[38]. Anomalous data for the Pt derivatives were collected at a wavelength of 1.07 Å. Heavy-metal positions for the *C*2 crystal form of StClC were identified by analysis of difference Patterson maps and by difference Fourier methods. Heavy-metal parameters were refined at 5 Å with SHARP[39]. SOLOMON was used for iterative solvent flattening and phase combination[40]. NCS operators were

© 2002 Macmillan Magazines Ltd

estimated with GETAX[41]. Two-fold averaging and phase extension to 4.5 Å with RAVE[42] allowed the building of a poly-alanine helix model, which served as a search model for molecular replacement into the $P2_12_12_1$ crystal form of EcClC using AMORE[43]. Phases in the $P2_12_12_1$ crystal form were extended to a resolution of 3.5 Å by six-fold NCS averaging with RAVE[42]. A model consisting of residues 12–461 was built into the averaged density using program O[44]. The locations of 17 methionine residues were identified by peaks ($>4\sigma$) in a $F_{Se}-F_{native}$ difference Fourier map. Refinement was carried out in several simulated annealing cycles using the maximum likelihood target implemented in CNS[45] followed by manual inspection and rebuilding of the molecule. Six-fold NCS constraints were used throughout refinement. Restrained individual *B*-factor refinement was justified by favourable observable-to-parameter ratio and a further drop of R_{free} (30.2%) and R_{cryst} (29.0%). The refined EcClC dimer was used as search model for molecular replacement into a $P2_1$ crystal form of StClC[43]. Four-fold NCS averaging and phase extension to 3.0 Å using RAVE[42] and DM[46] was followed by rebuilding of the model into the averaged electron density[44]. Initial cycles of simulated annealing refinement were carried out maintaining four-fold NCS constraints[45]. In later stages, the strict constraints were loosened within the two subunits of the dimer. The α-helix H–I loop, which differed in conformation between the two subunits of the same dimer, was rebuilt and the N terminus of subunit B was extended by 29 residues added onto α-helix A. These residues were not visible in subunit A. In further refinement cycles, the strict NCS constraints were maintained only between the two dimers in the asymmetric unit. Restrained, individual *B*-factors were refined. The final model has agreement factors R_{free} and R_{cryst} of 28.8% and 25.5%, respectively, and contains 6,574 protein atoms, two Cl^- ions, two sulphate ions (on the intracellular surface not near the pore), two lipids and one water. The presence of a halogen ion in the Cl^--binding site was confirmed with an $F_{Br}-F_{Cl}$ difference Fourier calculation in the StClC *C*2 crystal form.

Poisson–Boltzmann calculation

Electrostatic potential was calculated with DELPHI[47]. The ClC dimer, assigned a dielectric constant $\epsilon = 2$, was embedded in a membrane slab 18 Å thick ($\epsilon = 2$) and surrounded by water ($\epsilon = 80$, ionic strength 150 mM uni-univalent electrolyte). Partial protein charges were derived from the CHARMM 22 all-hydrogen force field[48]; hydrogen positions were generated with the program CNS[45]. Standard charging (neutral pH) was assumed for ionizable residues except Glu 235, which forms a carboxyl-carboxylate and therefore was uncharged. Electrostatic potential was calculated for a $99\times99\times99$ Å volume (grid spacing 0.8 Å).

Received 23 November; accepted 17 December 2001.

1. Doyle, D. A. *et al*. The structure of the potassium channel: molecular basis of K^+ conduction and selectivity. *Science* **280,** 69–77 (1998).
2. Zhou, Y., Cabral, J. M., Kaufman, A. & MacKinnon, R. Chemistry of ion coordination and hydration revealed by a K^+ channel–Fab complex at 2.0 Å resolution. *Nature* **414,** 43–48 (2001).
3. Jentsch, T. J., Friedrich, T., Schriever, A. & Yamada, H. The CLC chloride channel family. *Pflugers Arch.* **437,** 783–795 (1999).
4. Maduke, M., Miller, C. & Mindell, J. A. A decade of CLC chloride channels: structure, mechanism, and many unsettled questions. *Annu. Rev. Biophys. Biomol. Struct.* **29,** 411–438 (2000).
5. Fahlke, C. Ion permeation and selectivity in ClC-type chloride channels. *Am. J. Physiol. Renal Physiol.* **280,** F748–F757 (2001).
6. Steinmeyer, K., Lorenz, C., Pusch, M., Koch, M. C. & Jentsch, T. J. Multimeric structure of ClC-1 chloride channel revealed by mutations in dominant myotonia congenita (Thomsen). *EMBO J.* **13,** 737–743 (1994).
7. White, M. M. & Miller, C. A voltage-gated anion channel from the electric organ of *Torpedo californica*. *J. Biol. Chem.* **254,** 10161–10166 (1979).
8. Miller, C. Open-state substructure of single chloride channels from *Torpedo electroplax*. *Phil. Trans. R. Soc. Lond. B* **299,** 401–411 (1982).
9. Miller, C. & White, M. M. Dimeric structure of single chloride channels from *Torpedo electroplax*. *Proc. Natl Acad. Sci. USA* **81,** 2772–2775 (1984).
10. Jentsch, T. J., Steinmeyer, K. & Schwarz, G. Primary structure of *Torpedo marmorata* chloride channel isolated by expression cloning in *Xenopus* oocytes. *Nature* **348,** 510–514 (1990).
11. Ludewig, U., Pusch, M. & Jentsch, T. J. Two physically distinct pores in the dimeric ClC-0 chloride channel. *Nature* **383,** 340–343 (1996).
12. Middleton, R. E., Pheasant, D. J. & Miller, C. Homodimeric architecture of a ClC-type chloride ion channel. *Nature* **383,** 337–340 (1996).
13. Weinreich, F. & Jentsch, T. J. Pores formed by single subunits in mixed dimers of different CLC chloride channels. *J. Biol. Chem.* **276,** 2347–2353 (2001).
14. Maduke, M., Pheasant, D. J. & Miller, C. High-level expression, functional reconstitution, and quaternary structure of a prokaryotic ClC-type chloride channel. *J. Gen. Physiol.* **114,** 713–722 (1999).
15. Mindell, J. A., Maduke, M., Miller, C. & Grigorieff, N. Projection structure of a ClC-type chloride channel at 6.5 Å resolution. *Nature* **409,** 219–223 (2001).
16. White, M. M. & Miller, C. Probes of the conduction process of a voltage-gated Cl^- channel from *Torpedo electroplax*. *J. Gen. Physiol.* **78,** 1–18 (1981).
17. Rychkov, G. Y., Pusch, M., Roberts, M. L., Jentsch, T. J. & Bretag, A. H. Permeation and block of the skeletal muscle chloride channel, ClC-1, by foreign anions. *J. Gen. Physiol.* **111,** 653–665 (1998).
18. Rychkov, G., Pusch, M., Roberts, M. & Bretag, A. Interaction of hydrophobic anions with the rat skeletal muscle chloride channel ClC-1: effects on permeation and gating. *J. Physiol.* **530,** 379–393 (2001).
19. Richard, E. A. & Miller, C. Steady-state coupling of ion-channel conformations to a transmembrane ion gradient. *Science* **247,** 1208–1210 (1990).
20. Pusch, M., Ludewig, U., Rehfeldt, A. & Jentsch, T. J. Gating of the voltage-dependent chloride channel CIC-0 by the permeant anion. *Nature* **373,** 527–531 (1995).
21. Chen, T. Y. & Miller, C. Nonequilibrium gating and voltage dependence of the ClC-0 Cl^- channel. *J. Gen. Physiol.* **108,** 237–250 (1996).
22. Ludewig, U., Jentsch, T. J. & Pusch, M. Inward rectification in ClC-0 chloride channels caused by mutations in several protein regions. *J. Gen. Physiol.* **110,** 165–171 (1997).
23. Ludewig, U., Jentsch, T. J. & Pusch, M. Analysis of a protein region involved in permeation and gating of the voltage-gated *Torpedo* chloride channel ClC-0. *J. Physiol.* **498** (part 3), 691–702 (1997).
24. Maduke, M., Williams, C. & Miller, C. Formation of CLC-0 chloride channels from separated transmembrane and cytoplasmic domains. *Biochemistry* **37,** 1315–1321 (1998).
25. Maduke, M., Pheasant, D. J. & Miller, C. High-level expression, functional reconstitution, and quaternary structure of a prokaryotic ClC-type chloride channel. *J. Gen. Physiol.* **114,** 713–722 (1999).
26. Kleywegt, G. J. & Read, R. J. Not your average density. *Structure* **5,** 1557–1569 (1997).
27. Cowan, S. W. *et al*. Crystal structures explain functional properties of two *E. coli* porins. *Nature* **358,** 727–733 (1992).
28. Murata, K. *et al*. Structural determinants of water permeation through aquaporin-1. *Nature* **407,** 599–605 (2000).
29. Fu, D. *et al*. Structure of a glycerol-conducting channel and the basis for its selectivity. *Science* **290,** 481–486 (2000).
30. Grigorieff, N., Ceska, T. A., Downing, K. H., Baldwin, J. M. & Henderson, R. Electron-crystallographic refinement of the structure of bacteriorhodopsin. *J. Mol. Biol.* **259,** 393–421 (1996).
31. Fahlke, C., Yu, H. T., Beck, C. L., Rhodes, T. H. & George, A. L. Jr Pore-forming segments in voltage-gated chloride channels. *Nature* **390,** 529–532 (1997).
32. Fahlke, C., Beck, C. L. & George, A. L. Jr A mutation in autosomal dominant myotonia congenita affects pore properties of the muscle chloride channel. *Proc. Natl Acad. Sci. USA* **94,** 2729–2734 (1997).
33. Roux, B. & MacKinnon, R. The cavity and pore helices in the KcsA K^+ channel: electrostatic stabilization of monovalent cations. *Science* **285,** 100–102 (1999).
34. Andersen, O. S. & Fuchs, M. Potential energy barriers to ion transport within lipid bilayers. *Biophys. J.* **15,** 795–830 (1975).
35. McLaughlin, S. Electrostatic potentials at membrane-solution interfaces. *Curr. Top. Membr. Transp.* **9,** 71–144 (1977).
36. Jordan, P. C. Electrostatic modeling of ion pores. II. Effects attributable to the membrane dipole potential. *Biophys. J.* **41,** 189–195 (1983).
37. Otwinowski, Z. & Minor, W. Processing of X-ray diffraction data collected in oscillation mode. *Methods Enzymol.* **276,** 307–326 (1997).
38. Collaborative Computational Project No. 4. The CCP4 Suite: Programs for X-ray crystallography. *Acta Crystallogr. D* **50,** 760–763 (1994).
39. de La Fortelle, E. & Bricogne, G. in *Methods in Enzymology* (eds Carter, C. W. & Sweet, R. M.) 472–494 (Academic, New York, 1997).
40. Abrahams, J. P. & Leslie, A. G. W. Methods used in the structure determination of bovine mitochondrial F1 ATPase. *Acta Crystallogr. D* **52,** 30–42 (1996).
41. Vonrhein, C. & Schulz, G. E. Locating proper non-crystallographic symmetry in low-resolution electron-density maps with the program GETAX. *Acta Crystallogr. D. Biol. Crystallogr.* **55** (part 1), 225–229 (1999).
42. Kleywegt, G. J. & Jones, T. A. in *Proc. CCP4 Study Weekend* (eds Bailey, S.. Hubbard, R. & Waller, D.) 59–66 (Daresbury Laboratory, Daresbury, UK, 1994).
43. Navaza, J. AMoRe: an automated package for molecular replacement. *Acta Crystallogr. A* **50,** 157–163 (1994).
44. Jones, T. A., Zou, J. Y., Cowan, S. W. & Kjeldgaard, M. Improved methods for building protein models in electron density maps and the location of errors in these models. *Acta Crystallogr. A* **47,** 110–119 (1991).
45. Brunger, A. T. *et al*. Crystallography & NMR system: new software suite for macromolecular structure determination. *Acta Crystallogr. D* **54,** 905–921 (1998).
46. Cowtan, K. DM: an automated procedure for phase improvement by density modification. *Joint CCP4 ESF-EACBM Newslett. Protein Crystallogr.* **31,** 34–38 (1994).
47. Rocchia, W. *et al*. Rapid grid-based construction of the molecular surface and the use of induced surface charge to calculate reaction field energies: Application to the molecular systems and geometric objects. *J. Comp. Chem.* **23,** 128–137 (2002).
48. MacKerell, A. D. J. *et al*. All-atom empirical potential for molecular modeling and dynamics studies of proteins. *J. Phys. Chem. B* **102,** 3586–3616 (1998).
49. Thompson, J. D., Higgins, D. G. & Gibson, T. J. CLUSTAL W: improving the sensitivity of progressive multiple sequence alignment through sequence weighting, positions-specific gap penalties and weight matrix choice. *Nucleic Acids Res.* **22,** 4673–4680 (1994).
50. Sanner, M. F., Olson, A. J. & Spehner, J. C. Reduced surface: an efficient way to compute molecular surfaces. *Biopolymers* **38,** 305–320 (1996).

Supplementary Information accompanies the paper on *Nature*'s website (http://www.nature.com).

Acknowledgements

We thank M. Becker and L. Berman at the National Synchrotron Light Source X-25, the staff at the Cornell High Energy Synchrotron Source A1 and F1, and C. Petosa and A. Perrakis of the European Molecular Biology Laboratory at the European Synchrotron Radiation Facility ID-13 for assistance in data collection; J. Bonanno for technical assistance; members of the MacKinnon laboratory for assistance at all stages of the project; and S. Harrison, D. Jeruzalmi, A. Phillippsen and O. Andersen for discussions. This work was supported by grants from the National Institutes of Health (NIH) to R.M. and from the National Center for Research Resources, NIH, to B.T.C. R.M. is an investigator in the Howard Hughes Medical Institute.

Competing interests statement

The authors declare that they have no competing financial interests.

Correspondence and requests for materials should be addressed to R.M. (e-mail: mackinn@rockvax.rockefeller.edu). Coordinates have been deposited with the Protein Data Bank under accession codes 1KPK and 1KPL.

© 2002 Macmillan Magazines Ltd